Arabian Journal for Science and Engineering (2024) 49:753–764
https://doi.org/10.1007/s13369-023-08495-0

RESEARCH ARTICLE-CHEMISTRY

Biogenic ZnO/CuO/Fe_2O_3 Nanocomposite: A Groundbreaking Approach for Enhanced Degradation Capabilities and Reusability in Dye Removal Applications

Abdelghani Serouti[1,2] · Laouini Salah Eddine[1] · Souhaila Meneceur[1] · Gamil Gamal Hasan[1] · Hamdi Ali Mohammed[1] · Chaima Salmi[1] · Kir Iman[1] · Mohammed Fouad Ferhat[1,2,3] · Ouarda Ben Ali[4] · Johar Amin Ahmed Abdullah[5]

Received: 6 July 2023 / Accepted: 6 November 2023 / Published online: 30 November 2023

Abstract

We present the successful synthesis of a biogenic ZnO/CuO/Fe_2O_3 nanocomposite using an aqueous leaf extract of *Ocimum Basilicum L*. The confirmation of biosynthesis was achieved through UV–Visible spectrophotometry (UV–Vis), which provided evidence of ZnO/CuO/Fe_2O_3 NC formation. Scanning Electron Microscopy further confirmed the nanoscale size of the NC, measuring at 65 nm. X-Ray Diffraction analysis revealed a hexagonal structure for ZnO and a monoclinic structure for CuO. The successful synthesis of the environmentally friendly ZnO/CuO/Fe_2O_3 NC was further verified using Fourier transformed infrared (FT-IR) spectroscopy, which identified the functional groups present in the composite. Notably, the ZnO/CuO/Fe_2O_3 NC demonstrated exceptional degradation capabilities for toluidine blue (TB), p-toluidine (PT), and m-Toluidine (MT), with degradation rates of 99%, 99.1%, and 99.7%, respectively, within a reaction time of 120 min. The reaction kinetics followed a pseudo-first order model, with rate constant (k) values of 0.0314 min^{-1} and 0.0189 min^{-1} for TB and PT, respectively. This high rate of dye degradation can be attributed to the low band gap of the NC, which was determined to be 1.44 eV for the indirect bandgap. Furthermore, the nanocomposite exhibited excellent degradation reusability, maintaining a high degradation rate in each cycle.

Keywords Metal oxide nanoparticles · Zinc · Copper · Iron · Dyes degradation · Photocatalytic · Reusability

1 Introduction

Nanocomposites containing metal oxides are currently a significant research topic due to their high efficiency in features of sustainable development, the lack of secondary contamination during water treatment, and photocatalytic degradation [1–3]. Wastewater, which contains large quantities of harmful pollutants for the environment, is of particular research interest. Due to their high reactivity, vast surface area, functionalization, and effectiveness, nanoparticles are employed for the treatment and purification of wastewater [4–6]. Among the methods used to treat water, adsorption is considered effective because of its low cost, high efficiency, and effectiveness [7–10]. Wastewater cannot be sufficiently treated using conventional water treatment methods such as coagulation, flocculation, bed filtration, membrane filtration, precipitation, biodegradation, and oxidation [11–14]. Adsorption has been shown to be preferable to several other procedures since it is straightforward, impervious to dangerous pollutants, and adaptable [15–17]. Industries such as petrochemicals, paper, pulp, food, and textiles produce many different types of sanitary waste. Among the pollutants of concern are organic dyes, including Toluidine blue (TB), p-toluidine (PT), and m-Toluidine (MT), which

✉ Johar Amin Ahmed Abdullah
jabdullah@us.es

1 Department of Process Engineering, Faculty of Technology, University of El Oued, 39000 El Oued, Algeria

2 Laboratory of Sciences and Techniques of the Environment and Valorization, University of Abdelhamid Benbbadis of Mostaganem, BP 227, 27000 Mostaganem, Algeria

3 Unit of Renewable Energy Development in Arid Zones (UDERZA), El-Oued University, El Oued, Algeria

4 Department of Chemistry, Faculty of Exact Science, El Oued University, 39000 El Oued, Algeria

5 Department of Chemical Engineering, Higher Polytechnic School, University of Seville, 41011 Seville, Spain

are commonly found in industrial wastewater effluents [18, 19]. These dyes are used extensively in industries such as textiles, pharmaceuticals, and petrochemicals, but their improper disposal poses significant environmental risks [20]. TB, PT, and MT are known to be persistent and hazardous pollutants, often requiring advanced treatment methods for effective removal. Conventional water treatment processes may fall short in adequately treating these complex organic compounds. Hence, the development of advanced materials like our ZnO/CuO/Fe_2O_3 nanocomposite holds substantial promise in addressing the challenges posed by these recalcitrant dye pollutants.

Nanoparticle synthesis can generally be achieved using two primary approaches: physical methods or chemical and biological methods. Nevertheless, employing physical and chemical techniques for nanoparticle synthesis comes with certain disadvantages, including high expenses, toxicity, and environmental hazards [21]. Consequently, scientists have been exploring the potential of biological methods for producing nanoparticles. Biogenic sources, such as plants, actinomycetes, microorganisms, fungi, and algae, have been employed in the biological production of nanoparticles [22]. Recent research has suggested that plant extracts offer a promising environmentally friendly alternative for nanomaterial production [23–28]. The active components found in plant extracts, such as enzymes, polyphenols, phenolics, carbohydrates, and proteins, are effective in reducing, stabilizing, and encapsulating metal ions, leading to the creation of metal nanoparticles [29, 30]. Furthermore, nanoparticles generated from plants exhibit superior stability and consistency in terms of shape and size when compared to traditional chemical techniques [31]. In this context, the use of natural extracts as reducing and stabilizing agents in nanocomposite synthesis has emerged as an innovative and eco-conscious approach. Among the various plant extracts, the *Ocimum Basilicum*, or basil, extract holds particular promise. *Ocimum Basilicum* is renowned for its rich phytochemical composition, containing a wealth of bioactive compounds that can facilitate the reduction and capping of metal ions during nanocomposite synthesis [29]. Furthermore, its availability and ease of extraction make it an attractive candidate for sustainable materials production [32–34]. In this study, we harness the potential of *Ocimum Basilicum* leaf extract to synthesize a biogenic ZnO/CuO/Fe_2O_3 nanocomposite, highlighting the importance of green synthesis and the unique properties of this botanical agent in advancing nanomaterials for various applications.

Zinc oxide (ZnO) is an active and interesting material in photocatalytic applications, and it has been extensively studied due to its diverse physical and chemical properties [35–37]. In the field of photocatalytic processes, zinc oxide has emerged as a primary candidate due to its unique characteristics, such as low cost, easy accessibility to raw materials, non-toxicity, and good thermal and chemical stability [38]. The reported photocatalytic activity, however, may be greatly influenced by the shape and size of the used zinc oxide nanostructures [39, 40]. It is well known that low-dimensional zinc oxide structures, such as one-dimensional structures, have large surfaces, efficient carrier migration, and short charge carrier migration paths, all of which increase the photocatalytic activity [41, 42]. In other words, the characteristics and possible uses of low-dimensional zinc oxide nanocrystals can be determined by their carefully regulated composition and the precisely specified shape of various exposed crystal faces (i.e., polar and non-polar faces with variable energies on the surface) [43, 44].

The commercial use of zinc oxide in solar photocatalysis still has a number of limitations, including the broad bandgap, fast recombination of the photo-generated charge carrier, and the catalyst's corrosion and dissolution under harsh acidic conditions [45]. These problems can be resolved either by utilizing porous support materials to enhance the surface area by forming internal spaces for mass transfer or by combining zinc oxide with the other metal oxides to reduce the rate of recombination of photo-generated electrons and holes [46–48]. To address these problems, techniques have been reported, such as coupling with other photocatalysts, surface modification, ion, doping, dye improvement, integration into porous materials, and metal or non-metal doping, as the most effective approaches in the literature [49, 50]. Among these methods, the combination of zinc oxide with narrow bandgap semiconductors such as Fe_2O_3, $CoFe_2O_4$, WO_3, CuS, In_2O_3, Bi_2O_3, g-C_3N_4, Fe_3O_4, and CuO can enhance the photocatalytic activity of zinc oxide by reducing the recombination of light-induced charge carriers [51].

Therefore, this study addresses the critical need for the development of advanced composite materials by exploring the novel approach of combining multiple functional composites. The aim is to enhance their properties and unlock new possibilities for various applications. In this research, we present a groundbreaking method for synthesizing a biogenic ZnO/CuO/Fe_2O_3 nanocomposite using an aqueous leaf extract of *Ocimum Basilicum L*. This innovative synthesis approach offers several advantages, including its environmentally friendly nature, sustainability, and avoidance of hazardous chemicals. The synthesized ZnO/CuO/Fe_2O_3 nanocomposite underwent a comprehensive characterization process, including UV–Visible spectrophotometry, SEM analysis, and XRD analysis, providing valuable insights into its optical properties, nanoscale size, morphology, and crystal structures. The combination of multiple functional composites in this nanocomposite offers exciting prospects for enhanced performance and diverse applications. The findings of this research hold significant importance for advancing composite materials and their utilization in various fields,

including environmental remediation and multiple industries.

2 Materials and Methods

2.1 Materials

Ocimum Basilicum L. were collected from east Algeria. Iron (III) chloride ($FeCl_3$, 98%), zinc chloride ($ZnCl_2$, 98%), copper (II) chloride hydrate ($CuCl_2$-$2H_2O$, 98%), sodium hydroxide (NaOH, 98%), were purchased from Sigma-Aldrich, Germany.

2.2 Preparation of the Extract

The plant extract was prepared by collecting leaves of the *Ocimum Basilicum* plant. The leaves were cleaned using tap water to remove any dirt particles, followed by multiple washes with distilled water. A total of 200 g of the cleaned leaves was weighed and placed in a glass beaker with 1000 mL of distilled water. The mixture was left to sit overnight. The next day, the extract was filtered to remove any solid residues and transferred to a bottle. Finally, the bottle containing the extract was stored at a low temperature to ensure its quality and stability.

2.3 Synthesis of ZnO/CuO/Fe_2O_3 Nanocomposites by Green Method

To synthesize the ZnO/CuO/Fe_2O_3 nanocomposites, a mixture containing 8.2 g of $FeCl_3$, 2.8 g of $ZnCl_2$, and 8.2 g of $CuCl_2{\cdot}2H_2O$ was combined with the prepared *Ocimum Basilicum* extract. The resulting mixture was subjected to continuous stirring and heating at 75 °C for approximately three hours. During this process, drops of NaOH (2 M) were added incrementally to adjust the solution's acidity until a noticeable change in color occurred, leading to the formation of a brown precipitate. To separate the precipitate, a centrifuge was employed, operating at a speed of 3000 rpm for a duration of 5 min. The obtained precipitate was then subjected to multiple washes using distilled water (DW) to eliminate impurities. Subsequently, the wet powder was dried by placing it in an oven set at 80 °C overnight. To obtain the final ZnO/CuO/Fe_2O_3 nanocomposite, the dried powder underwent annealing in an oven at a temperature of 500 °C for a duration of 3 h. This process facilitated the formation and stabilization of the desired nanocomposite structure. The experimental procedure for preparing the ZnO/CuO/Fe_2O_3 nanocomposite.

2.4 Characterization ZnO/CuO/Fe_2O_3 Nanocomposite

The UV–visible spectrophotometer (SECOMAM, model 9600, France) was employed to assess the optical properties within the wavelength range of 200–800 nm. To investigate the crystalline nature of the ZnO/CuO/Fe_2O_3 nanocomposite, XRD analysis was performed using the Proto Manufacturing Company's Benchtop model XRD machine (USA). The Fourier transform infrared spectroscopy (FTIR) technique was utilized (Thermo Fisher Scientific, Nicolet iS5 model, USA) to confirm the functional groups present in the nanocomposites. Additionally, a scanning electron microscope (TESCAN, VEGA3 model, USA) was utilized to examine the particle size and shape. The crystallite size was determined using the Scherrer formula (Eq. 1), where a prominent peak with the highest intensity was selected. The formula is as follows [52]:

$$D = \frac{k\lambda}{\beta \cos\theta} \tag{1}$$

Here "k" represents the form factor (0.9), "D" represents the crystallite size (0.15418 nm, CuK), "β" denotes the Full Width at Half Maximum (FWHM), and "θ" represents the diffraction angle.

2.5 Photocatalytic Activity of ZnO/CuO/Fe_2O_3 Nanocomposite

The degradation of Toluidine blue (TB), p-toluidine (PT) and m-Toluidine (MT) under sunlight at 29 °C, was studied using the nanocomposite as a photocatalyst. An aqueous solution containing the dyes at a concentration of 2.5×10^{-5} M of TB, p-toluidine and m-Toluidine was used. 5 ml of each dye was placed separately in several beakers and 5 mg of ZnO/CuO/Fe_2O_3 was added. The resulting mixture was then irradiated under sunlight for 0, 15, 30, 45, 60, 75, 90 and 105 min. ZnO/CuO/Fe_2O_3 was separated from the solution using a photocatalyst powder removal centrifuge. The degradation activity was investigated in March 2023 and the average sunlight intensity was about 29 °C in El Oued, Algeria. The absorbance of dye was analyzed through UV–Vis spectrophotometry in the range of 200–900 nm. The percentage of hydrolysis of each dye was calculated using the following equation [53].

$$\%degradation = \frac{A_0 - A_{(t)}}{A_0} \times 100 \tag{2}$$

where A_0 is the measured absorbance of dye solutions without the catalyst nanocomposite, $A_{(t)}$ is the measured absorbance when the catalyst is added after each time periods.

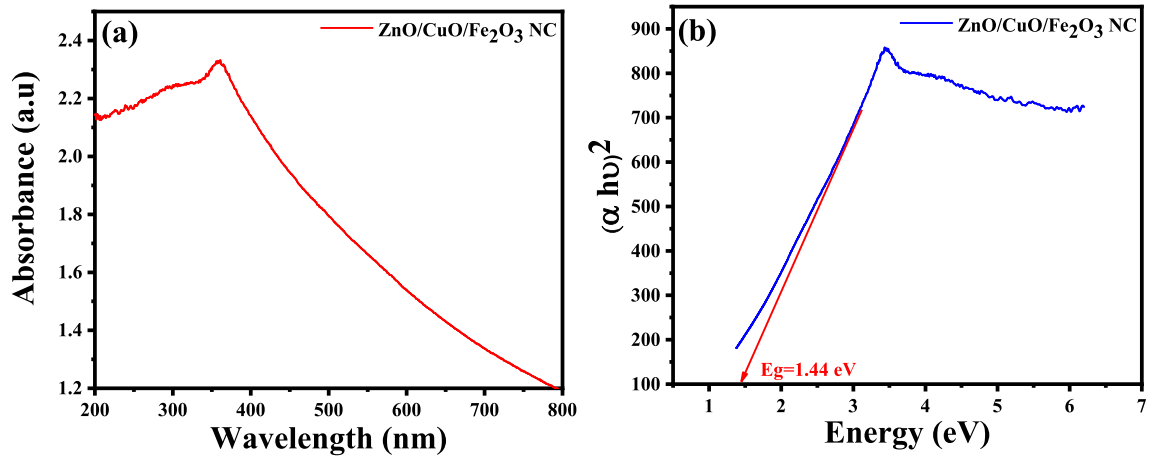

Fig. 1 **a** UV–Vis absorption spectra of ZnO/CuO/Fe_2O_3 NC, **b** Energy dependence of $(\alpha h\nu)^2$ for ZnO/CuO/Fe_2O_3 NC

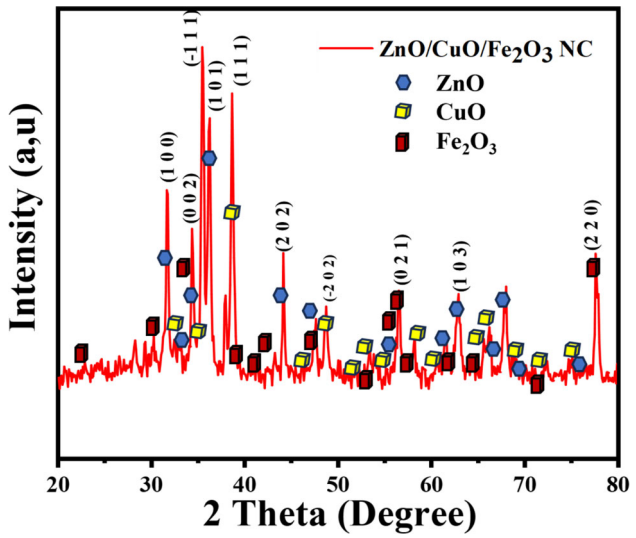

Fig. 2 XRD patterns of ZnO/CuO/Fe_2O_3 NC

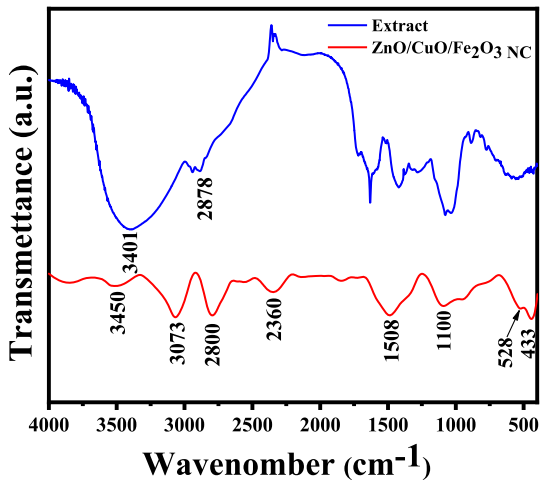

Fig. 3 FTIR spectra of ZnO/CuO/Fe_2O_3 NC (red) and *Ocimum Basilicum* extract (blue)

3 Results and Discussion

3.1 Optical Characteristics and Band Gap Energy

Figure 1 illustrates the UV–Vis absorption spectra of the ZnO/CuO/Fe_2O_3 nanocomposite, providing valuable insights into its optical properties.

In Fig. 1a, the absorption spectrum in the visible range reveals a peak at $\lambda_{max} = 360.9$ nm. This indicates that the nanocomposite is capable of absorbing light in the visible region, suggesting its potential for various optoelectronic applications. Furthermore, the band gap energy of the ZnO/CuO/Fe_2O_3 nanocomposite was determined using the $(\alpha h\nu)^2$ versus energy function (eV) plot, as shown in Fig. 1b. By analyzing the data, the band gap energy was estimated to be 1.44 eV. The band gap energy is a crucial parameter in determining the semiconductor behavior and optical properties of materials. The obtained value of 1.44 eV indicates that the nanocomposite possesses a suitable band gap for absorbing light in the visible range. The successful synthesis of the ZnO/CuO/Fe_2O_3 nanocomposite is supported by the observed absorption in the visible spectrum and the determined band gap energy. These findings highlight the potential of the nanocomposite for applications such as photocatalysis, photovoltaics, and sensor technologies, where efficient light absorption and charge carrier generation are essential.

3.2 XRD Analysis

As shown in Fig. 2, the XRD pattern showed multiple peaks of the produced ZnO/CuO/Fe_2O_3 NC.

The broad peaks show that the material as it was produced comprises nanoscale-sized particles. The 2θ angles corresponding to the diffraction peaks are as follows: 31.779°,

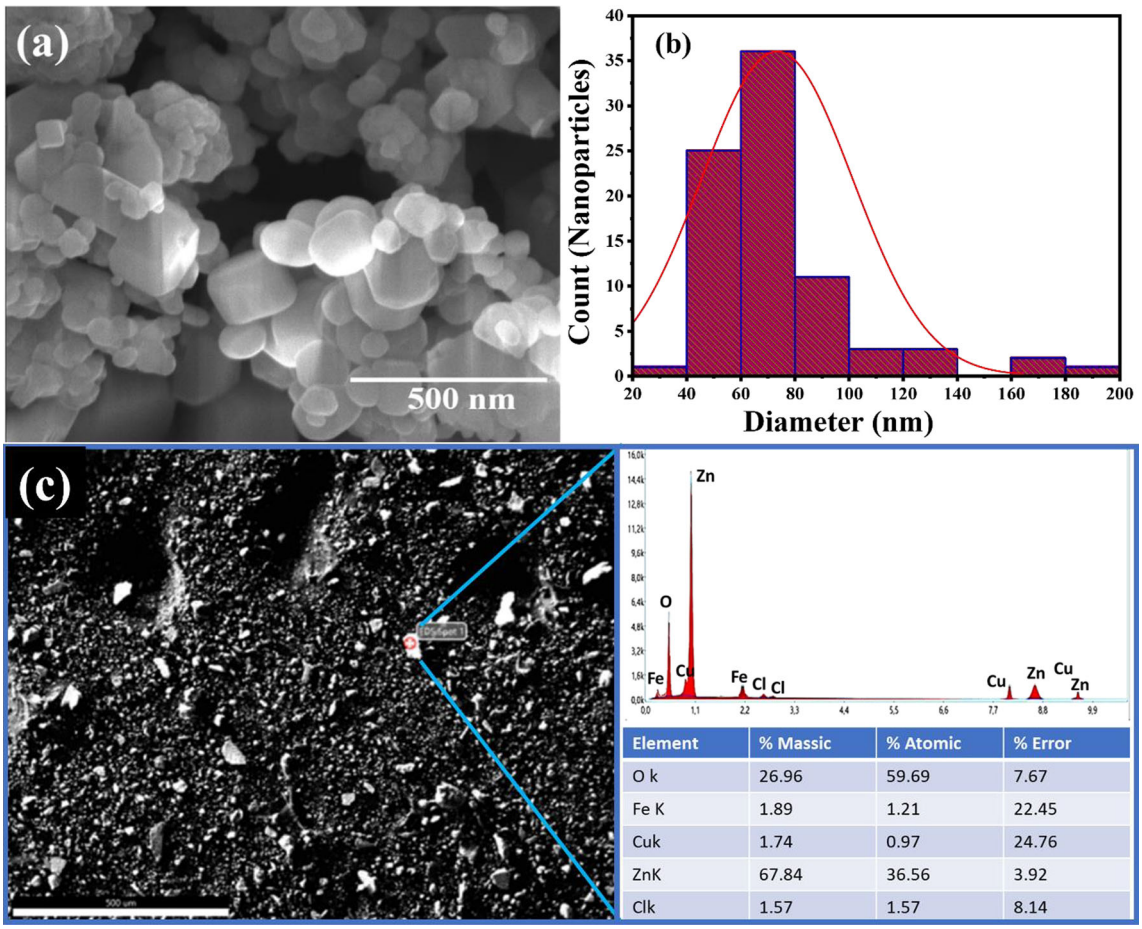

Element	% Massic	% Atomic	% Error
O k	26.96	59.69	7.67
Fe K	1.89	1.21	22.45
Cuk	1.74	0.97	24.76
ZnK	67.84	36.56	3.92
Clk	1.57	1.57	8.14

Fig. 4 SEM images of bio-synthesized ZnO/CuO/Fe_2O_3 nanocomposite. **a** Representative SEM image showing the morphology of the nanocomposite. **b** Size distribution analysis providing information about the particle size distribution. **c** EDX result and elemental analysis highlighting the presence of different elements in the nanocomposite

34.430°, 36.265°, 47.554°, 56.615°, 62.876°, 66.400°, 67.971°, 69.112°, 72.587°, and 76.988°. These angles correspond to the crystallographic planes (1 0 0), (0 0 2), (1 0 1), (1 0 2), (1 1 0), (1 0 3), (2 0 0), (1 1 2), (2 0 1), (0 0 4), and (2 0 2), respectively. These observations indicate that the ZnO NPs possess a hexagonal crystal structure with a space group of P63mc (186) and lattice parameters of a = 3.2495 Å and c = 5.2069 Å, as specified in JCDPS Card No. 01-089-0510. Additionally, the presence of the CuO NPs was confirmed by the XRD spectrum, which included peaks other than the normal ZnO/CuO/Fe_2O_3 peaks at 2θ = 32,524°, 35,564°, 38,725°, 46,287°, 48,795°, 51,360°, 53,480°, 56,719°, 58,297°, 61,582°, 65,816°, 66,528°, 68,120°, 68,923°, 72,424°, 72,963°, 75,032°, corresponding to crystallographic reflection planes (1 1 0), (−1 1 1), (1 1 1), (−1 1 2), (−2 0 2), (1 1 2), (0 2 0), (0 2 1), (2 0 2), (−1 1 3), (0 2 2), (3 1 0), (2 2 0), (−2 2 1), (3 1 1), (2 2 1) and (0 0 4) respectively, where CuO NPs had a monoclinic crystal structure (Space group C2/c (15) and lattice parameters of a = 4,6830 Å b = 3,4240 Å and c = 5,1290 Å) JCDPS Card No. 01-089-5896. Furthermore, the XRD spectrum revealed peaks other than the typical Fe_2O_3 peaks, confirming the presence of the ZnO/CuO/Fe_2O_3 complex at 2θ = 23,851°, 32,856°, 35,080°, 39,076°, 40,321°, 42,866°, 48,823°, 53,511°, 55,254°, 56,544°, 57,194°, 61,527°, 62,931°, 65,114°, 68,891°, 71,636°, and 74,133°, corresponding to crystallographic reflection planes (0 1 2), (1 0 4), (1 1 0), (0 0 6), (1 1 3), (2 0 2), (0 2 4), (1 1 6), (2 1 1), (1 2 2), (0 1 8), (2 1 4), (3 0 0), (1 2 5), (2 0 8), (1 1 9), (2 2 0) respectively, where Fe_2O_3 NPs had a rhombohedral crystal structure (Space group R-3c (167) and lattice parameters of a = 5,1120 Å b = 5,1120 Å and c = 13,8200 Å) JCDPS Card No. 088-2359. The crystallite sizes of the ZnO/CuO/Fe_2O_3 nanocomposite sample were 29.1 nm, according to the Scherrer formula.

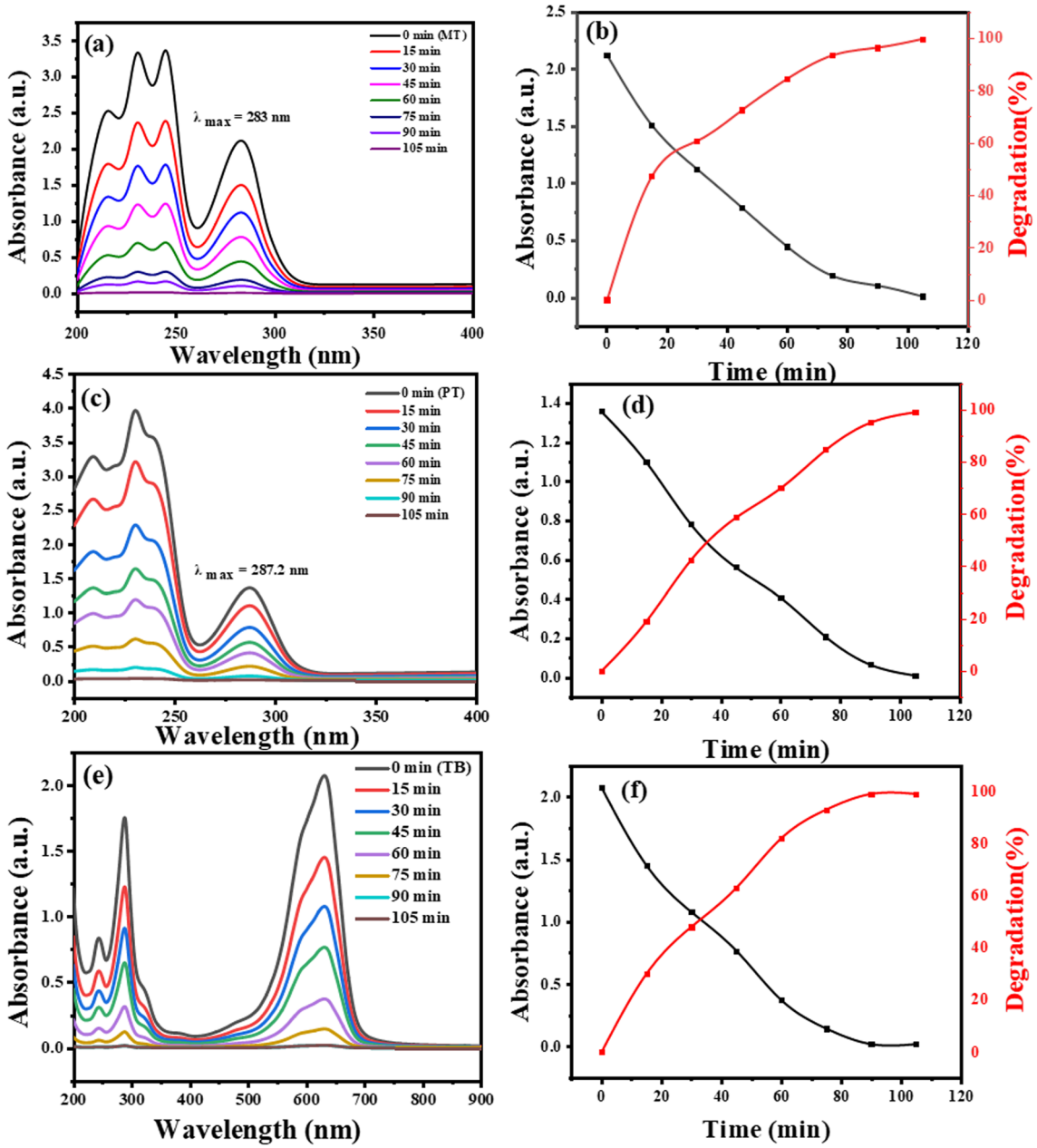

Fig. 5 Photodegradation efficiency versus reaction time: UV–vis spectra for the degradation of **a** MT dye, **c** PT dye, and **e** TB dye using ZnO/CuO/Fe_2O_3 NC. The degradation rate of **b** MT dye, **d** PT dye, and **f** TB dye using ZnO/CuO/Fe_2O_3 NC

3.3 FTIR Analysis

The FT-IR studies of *Ocimum Basilicum* leaf extract and synthesized ZnO/CuO/Fe_2O_3 nanocomposite are given in Fig. 3.

The FTIR analysis was performed to determine the purity and nature of the nanoparticles, as well as the existence of phytochemicals in the extract. The FTIR spectrum at around 3400–3800 cm^{-1} for the *Ocimum Basilicum* extract could be attributed to the hydroxyl of the phenols stretching mode [54]. The O–H stretching vibrations could potentially account for the absorption peaks detected within the range of 3200–3500 cm^{-1} in the spectrum of the ZnO/CuO/Fe_2O_3 nanocomposite [55]. The peaks around 2360 cm^{-1} and 3073 cm^{-1} are the H–O–H vibration of a cluster of crystallized water molecules and C–H stretching, respectively [56, 57]. The peak at 1508 cm^{-1} was likely due to C=O [57]. The stretching vibration of C–O–C is responsible for the band observed at 1100 cm^{-1} in both extract and ZnO/CuO/Fe_2O_3 nanocomposite spectrum. Furthermore, the peaks detected at 2878 cm^{-1} were assigned to the stretching vibrations of the $–CH_2$ functional group [58]. According to related studies, the characteristic peaks of Fe–O in Fe_2O_3 were at

390–566 cm^{-1}, while the Cu–O stretching band in the monoclinic phase and the Zn–O stretching band were observed in 420–600 and 401–670 cm^{-1} regions, respectively [59–61].

3.4 Structure and Morphology

The morphological dimensions of the produced $ZnO/CuO/Fe_2O_3$ nanocomposites were investigated using SEM images (Fig. 4a).

The average size distribution of the biosynthesized $ZnO/CuO/Fe_2O_3$ nanocomposite is around 65 nm, as shown by the particles size distribution histograms in Fig. 4b. As shown, $ZnO/CuO/Fe_2O_3$ nanocomposite particles come in a variety of sizes and irregular forms. The performance of photocatalysis can be significantly influenced by the geometry of a material's surface. Figure 4c illustrates the EDX analysis of the ternary nanocomposite $ZnO/CuO/Fe_2O_3$, displaying the mass and atomic percentages of different elements. The embedded table summarizes these value percentages for easy reference. The higher mass and atomic percentages of oxygen (O) and zinc (Zn) indicate their dominant presence in the composition. This could be attributed to the synthesis method, or the nature of the starting materials used. Conversely, iron (Fe), copper (Cu), and chlorine (Cl) exhibit lower percentages in comparison. These findings provide insights into the elemental compositions of the nanocomposite. Figure 4c enhances the understanding of the composition by visually representing the higher percentages of oxygen (O) and zinc (Zn), as well as the lower percentages of iron (Fe), copper (Cu), and chlorine (Cl). This graphical overview complements the table, facilitating comparisons between different elements and contributing to a comprehensive understanding of the nanocomposite's composition.

3.5 Photocatalytic Activity Study

After the obtained results, this study confirmed the effectiveness of the nanocomposite in adsorption and photocatalysis in the decomposition of toluidine blue (TB), p-toluidine (PT) and m-Toluidine (MT) dyes under sunlight at normal atmospheric temperature. The intensity of the absorption peaks for all dyes used in this experiment decreased gradually with the increase in time without changing the maximum absorption wavelength. UV–Vis analysis revealed the absorption features at λ_{max} = 630.8 nm, 287.2 nm and 283 nm for TB, PT and MT, respectively. The results indicate that $ZnO/CuO/Fe_2O_3$ NPs have good disappearance efficacy TB, PT and MT dyes and showed a degradation rate of 99%, 99.1% and 99.7%, within 90 min, respectively (Fig. 5a, b, and e).

Kinetic studies, using a pseudo-first-order kinetic model, demonstrate the photocatalytic performance of the as-prepared photocatalysts (Eq. 3) [62] as shown in Fig. 5.

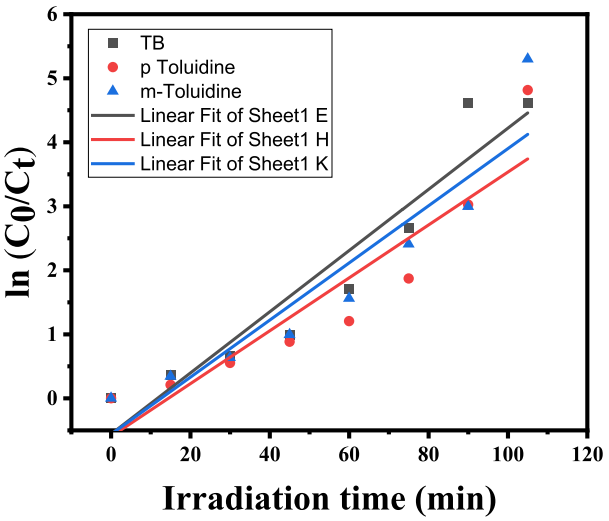

Fig. 6 Shows the first-order kinetic plot of $\ln(A_0/A_t)$ versus time for the degradation of MT, PT, and TB dyes using $ZnO/CuO/Fe_2O_3$ NC

Moreover, the rate constant of $ZnO/CuO/Fe_2O_3$ NC was estimated to be about 0.0314 min^{-1}, 0.0189 min^{-1} for TB, p-toluidine and m-Toluidine, respectively.

$$\ln\left(\frac{Ct}{C0}\right) = t \times k \tag{3}$$

where K is pseudo-first order rate constant, and t is irradiation time.

The photoremoval kinetics of the dyes was studied using pseudo-first-order kinetics. The degradation efficiency and rate constant for TB, p-toluidine and m-Toluidine were calculated from the reaction profiles and kinetic plots in Fig. 6 using the simple equations as follows:

$$R\% = \left(1 - \frac{Ct}{C0}\right) \times 100 \tag{4}$$

where R% is degradation efficiency of TB, p-toluidine and m-Toluidine, C_0 is the initial concentration and C_t is the concentration of days at different irradiation time.

3.6 Reusability and Stability Performance of $ZnO/CuO/Fe_2O_3$ Photocatalyst

The objective of this study was to investigate the stability and reusability of the $ZnO/CuO/Fe_2O_3$ nanocomposites, which was prepared for treating textile wastewater. This research also aimed to assess the applicability of the nanocomposite in industrial settings, considering sustainability and stability as important factors. In the initial cycle, a sample of the synthesized photocatalyst (20 mg) was added to a solution containing TB dye (2.5×10^{-5} M) in a volume of 20 mL.

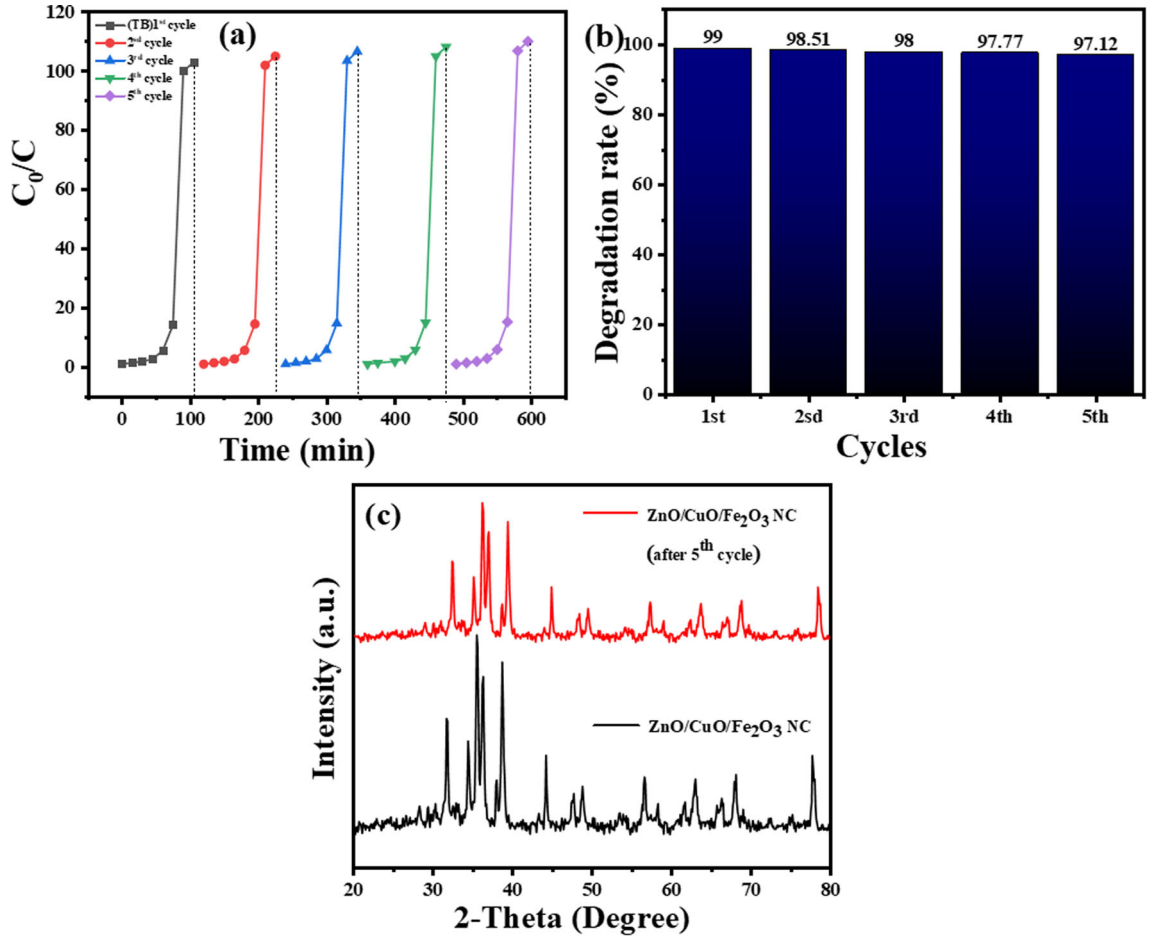

Fig. 7 **a** Recyclability of the $ZnO/CuO/Fe_2O_3$ photocatalyst for degradation of TB; **b** Reusability (degradation efficiency vs. number of cycles) of $ZnO/CuO/Fe_2O_3$ in the photodegradation of TB, respectively. **c** XRD analysis of $ZnO/CuO/Fe_2O_3$ and reused. The results demonstrated consistently high photocatalytic degradation efficiencies for the photocatalyst, indicating its excellent performance and comparability throughout the experiment. The X-ray diffraction (XRD) data depicted in Fig. 7c provide clear evidence that the crucial XRD diffraction peaks of the $ZnO/CuO/Fe_2O_3$ photocatalyst remained unaltered before and after the photodegradation process, even after undergoing five consecutive photocatalytic cycles. This observation signifies that the catalytic substance did not cause any changes in the diffraction peaks of the $ZnO/CuO/Fe_2O_3$ photocatalyst

Each solution was then exposed to sunlight for 105 min. Subsequently, the photocatalyst sample was separated from the solutions using filtration, washed multiple times with double distilled water, and dried in an oven at 60 °C for 4 h to remove any remaining moisture. The dried photocatalyst was reused in the subsequent cycles under the same experimental conditions as the first cycle. This process was repeated for five cycles, and the degradation efficiencies for each cycle, as well as the degradation percentages over time (C/C_0), are presented in Fig. 7a and b.

3.7 Photodegradation Mechanism of $ZnO/CuO/Fe_2O_3$

The degradation process of dyes in a solution is initiated by the catalyst's photoexcitation, which results in the generation of electron–hole pairs on the photocatalyst's surface (as shown in Eqs. 5–11) [63].

$$ZnO/CuO/Fe_2O_3 \xrightarrow{hv} e^-_{(CB)} + h^+_{(VB)} \quad (5)$$

$$e^-_{(CB)} \xrightarrow{ZnO/CuO/Fe_2O_3} o_2^{\cdot -} \quad (6)$$

$$h^+_{(VB)} + H_2O \xrightarrow{ZnO/CuO/Fe_2O_3} H^+ + OH^- \quad (7)$$

$$H^+ + O_2^{\cdot -} \rightarrow HO_2^{\cdot} \quad (8)$$

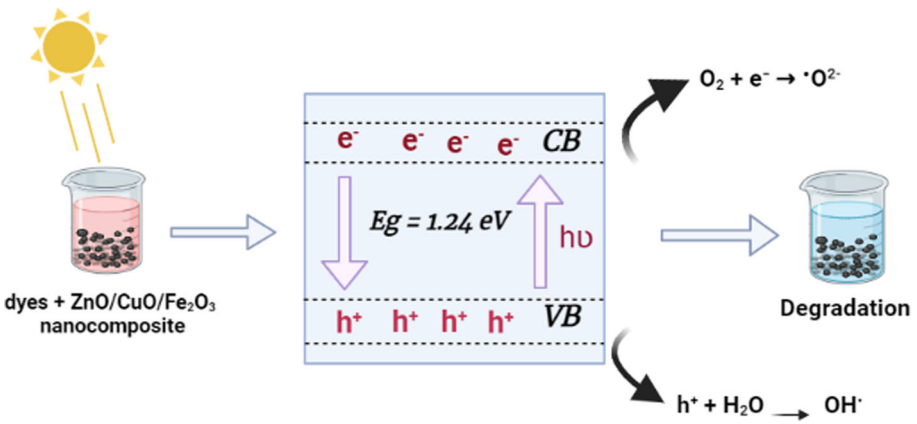

Fig. 8 Photocatalytic mechanism of $ZnO/CuO/Fe_2O_3$ NC

$$HO_2^{\cdot} + HO_2^{\cdot} \rightarrow H_2O_2 + O_2 \quad (9)$$

$$H_2O_2 \xrightarrow{hv} 2OH^{\cdot} \quad (10)$$

$$\text{Dyes} + OH^{\cdot} \xrightarrow{h^+} CO_2 + H_2O \quad (11)$$

The positively charged holes (h +) in the valence band (hVB +) possess a high oxidative potential, enabling the direct oxidation of dyes into reactive oxidative intermediates (as illustrated in Eq. (6)). The degradation of TB, for instance, involves the participation of OH• radicals, which are formed either by the decomposition of water or through the reaction of h + with OH − molecules, OH• radicals, although non-selective, are potent oxidants that facilitate the partial or complete mineralization of organic compounds. When $ZnO/CuO/Fe_2O_3$ nanocomposites are irradiated with visible light, they undergo photoexcitation via surface absorption, leading to the injection of photoexcited electrons into O_2. As a result, the production of superoxide and hydroxyl radicals is accelerated, ultimately enhancing the rate of degradation for dye molecules. The process of photocatalytic degradation of dyes using $ZnO/CuO/Fe_2O_3$ nanocomposite under solar radiation is shown in the following equations [64]. Figure 8 illustrates the mechanism behind the enhanced photocatalytic activity of $ZnO/CuO/Fe_2O_3$ nanocomposites under solar irradiation.

4 Conclusion

In conclusion, this study successfully synthesized a biogenic $ZnO/CuO/Fe_2O_3$ nanocomposite using an aqueous leaf extract of *Ocimum Basilicum L.* The confirmation of biosynthesis was achieved through UV–Visible spectrophotometry, which provided evidence of $ZnO/CuO/Fe_2O_3$ NC formation. SEM analysis confirmed the nanoscale size of the nanocomposite, measuring at 65 nm. XRD analysis revealed the hexagonal structure of ZnO and monoclinic structure of CuO. FT-IR spectroscopy verified the presence of functional groups in the composite. The $ZnO/CuO/Fe_2O_3$ NC exhibited exceptional degradation capabilities for various dyes, achieving high degradation rates within a short reaction time. The degradation followed a pseudo-first order model, with rate constant values indicating efficient degradation. The nanocomposite also demonstrated excellent degradation reusability. These findings highlight the potential of the environmentally friendly $ZnO/CuO/Fe_2O_3$ nanocomposite for various applications in wastewater treatment and environmental remediation.

Acknowledgements The authors would like to thank the Algerian Directorate General for Scientific Research and Technological Development-DGRSDT for financial assistance.

Author Contributions AS, LSE, and SM conceptualized the study. HAM, CS, and GGH developed the methodology. HAM and AS contributed to the software implementation. SM, KI, OBA, and LSE performed the validation. SM, GGH, AS, KI, MFF, and HAM conducted the formal analysis. KI, MFF, HAM, CS, and GGH were responsible for the investigation. SM and LSE provided the necessary resources. LSE curated the data. HAM, GGH, and OBA prepared the original draft of the manuscript. JAAA, and LSE contributed to the review and editing process. LSE handled the visualization. JAAA, SM, AS, and LSE supervised the study. SM and LSE. All authors have read and agreed to the published version of the manuscript.

Funding Funding for open access publishing: Universidad de Sevilla/CBUA. This research received no external funding.

Data Availability All data generated or analyzed during this study are included in this published article.

Declarations

Conflict of interest The authors declare no conflict of interest. The authors declare that they have no known competing financial interests or personal relationships that could have appeared to influence the work reported in this paper.

Ethics Approval Not applicable.

References

1. Kavil, J.; Alshahrie, A.; Periyat, P.: CdS sensitized TiO_2 nano heterostructures as sunlight driven photocatalyst. Nano-Struct. Nano-Objects **16**, 24–30 (2018)
2. Kir, I.; Laouini, S.E.; Meneceur, S.; Bouafia, A.; Mohammed, H.A.M.: Biosynthesis and characterization of novel nanocomposite ZnO/$BaMg_2$ efficiency for high-speed adsorption of AZO dye. Biomass Conv. Bioref. **26**, 1–36 (2023). https://doi.org/10.1007/s13399-023-03985-5
3. Althamthami, M.; Temam, E.G.; Temam, H.B.; Saad, R.; Hasan, G.G.: Improved photocatalytic activity under the sunlight of high transparent hydrophilic bi-doped TiO_2 thin-films. J. Photochem. Photobiol. A: Chem. **443**, 114818 (2023)
4. Zhan, F.; Yin, J.; Zhou, J.; Jiao, T.; Zhang, L.; Xia, M.; Bai, Z.; Peng, Q.: Facile preparation and highly efficient catalytic performances of Pd-Cu bimetallic catalyst synthesized via seed-mediated method. Nanomaterials **10**, 6 (2019)
5. Zhao, J.; Yin, J.; Zhong, J.; Jiao, T.; Bai, Z.; Wang, S.; Zhang, L.; Peng, Q.: Facile preparation of a self-assembled artemia cyst shell–TiO_2–MoS_2 porous composite structure with highly efficient catalytic reduction of nitro compounds for wastewater treatment. Nanotechnology **31**, 85603 (2019)
6. Kemp, K.; Griffiths, J.; Campbell, S.; Lovell, K.: An exploration of the follow-up up needs of patients with inflammatory bowel disease. J. Crohn's Colitis **7**, e386–e395 (2013)
7. Ajmal, S.; Bibi, I.; Majid, F.; Ata, S.; Kamran, K.; Jilani, K.; Nouren, S.; Kamal, S.; Ali, A.; Iqbal, M.: Effect of Fe and Bi doping on $LaCoO_3$ structural, magnetic, electric and catalytic properties. J. Mater. Res. Technol. **8**, 4831–4842 (2019)
8. Vickers, N.J.: Animal communication: when i'm calling you, will you answer too? Curr. Biol. **27**, R713–R715 (2017)
9. Jamil, A.; Bokhari, T.H.; Javed, T.; Mustafa, R.; Sajid, M.; Noreen, S.; Zuber, M.; Nazir, A.; Iqbal, M.; Jilani, M.I.: Photocatalytic degradation of disperse dye Violet-26 using TiO_2 and ZnO nanomaterials and process variable optimization. J. Mater. Res. Technol. **9**, 1119–1128 (2020)
10. Sohail, I.; Bhatti, I.A.; Ashar, A.; Sarim, F.M.; Mohsin, M.; Naveed, R.; Yasir, M.; Iqbal, M.; Nazir, A.: Polyamidoamine (PAMAM) dendrimers synthesis, characterization and adsorptive removal of nickel ions from aqueous solution. J. Mater. Res. Technol. **9**, 498–506 (2020)
11. Nagajyothi, P.C.; Vattikuti, S.V.P.; Devarayapalli, K.C.; Yoo, K.; Shim, J.; Sreekanth, T.V.M.: Green synthesis: photocatalytic degradation of textile dyes using metal and metal oxide nanoparticles-latest trends and advancements. Crit. Rev. Environ. Sci. Technol. **50**, 2617–2723 (2020)
12. Vasantharaj, S.; Sathiyavimal, S.; Palanisamy Senthilkumar, V.N.; Kalpana, G.R.; Alsehli, M.; Elfasakhany, A.; Pugazhendhi, A.: Enhanced photocatalytic degradation of water pollutants using biogreen synthesis of zinc oxide nanoparticles (ZnO NPs). J. Environ. Chem. Eng. **9**, 105772 (2021)
13. Hashmi, S.S.; Shah, M.; Muhammad, W.; Ahmad, A.; Ullah, M.A.; Nadeem, M.; Abbasi, B.H.: Potentials of phyto-fabricated nanoparticles as ecofriendly agents for photocatalytic degradation of toxic dyes and waste water treatment, risk assessment and probable mechanism. J. Indian Chem. Soc. **98**, 100019 (2021)
14. Huhtala, M.; Heino, J.; Casciari, D.; de Luise, A.; Johnson, M.S.: Integrin evolution: insights from ascidian and teleost fish genomes. Matrix Boil. **24**, 83–95 (2005)
15. Kakavandi, B.; Takdastan, A.; Pourfadakari, S.; Ahmadmoazzam, M.; Jorfi, S.: Heterogeneous catalytic degradation of organic compounds using nanoscale zero-valent iron supported on kaolinite: mechanism, kinetic and feasibility studies. J. Taiwan Inst. Chem. Eng. **96**, 329–340 (2019)
16. Ahmadi, M.; Niari, M.H.; Kakavandi, B.: Development of maghemite nanoparticles supported on cross-linked chitosan (γ-Fe2O3@ CS) as a recoverable mesoporous magnetic composite for effective heavy metals removal. J. Mol. Liq. **248**, 184–196 (2017)
17. Borna, M.O.; Pirsaheb, M.; Niri, M.V.; Mashizie, K.R.; Kakavandi, B.; Zare, M.R.; Asadi, A.: Batch and column studies for the adsorption of chromium (VI) on low-cost Hibiscus Cannabinus kenaf, a green adsorbent. J. Taiwan Inst. Chem. Eng. **68**, 80–89 (2016)
18. Zohra, R.; Meneceur, S.; Eddine, L.S.; Bouafia, A.; Mohammed, H.A.; Hasan, G.G.: Biosynthesis and characterization of MnO_2 and Zn/Mn_2O_4 NPs using Ziziphus spina-Christi aqueous leaves extract: effect of decoration on photodegradation activity against various organic dyes. Inorg. Chem. Commun. **156**, 111304 (2023)
19. Rabia, M.; Hadia, N.M.A.; Farid, O.M.; Abdelazeez, A.A.A.; Mohamed, S.H.; Shaban, M.: Poly (m-toluidine)/rolled graphene oxide nanocomposite photocathode for hydrogen generation from wastewater. Int. J. Energy Res. **46**, 11943–11956 (2022)
20. Okoro, H.K.; Pandey, S.; Ogunkunle, C.O.; Ngila, C.J.; Zvinowanda, C.; Jimoh, I.; Lawal, I.A.; Orosun, M.M.; Adeniyi, A.G.: Nanomaterial-based biosorbents: adsorbent for efficient removal of selected organic pollutants from industrial wastewater. Emerg. Contaminants **8**, 46–58 (2022)
21. Salmi, Chaima; Souhaila, Meneceur; Eddine, Laouini Salah; Mohammed, Hamdi Ali Mohammed.; Hasan, Gamil Gamal; Mahboub, Mohammed Sadok: Biosynthesis of Mn_3O_4/PVP nanocomposite for enhanced photocatalytic degradation of organic dyes under sunlight irradiation. J. Cluster Sci. (2023). https://doi.org/10.1007/s10876-023-02475-y
22. Manjari, G.; Saran, S.; Arun, T.; Devipriya, S.P.; Vijaya Bhaskara Rao, A.: Facile aglaia elaeagnoidea mediated synthesis of silver and gold nanoparticles: antioxidant and catalysis properties. J. Cluster Sci. **28**, 2041–2056 (2017)
23. Hasan, G.G.; Mohammed, H.A.; Althamthami, M.; Khelef, A.; Laouini, S.E.; Meneceur, S.: Synergistic effect of novel biosynthesis SnO_2@ Fe_3O_4 nanocomposite: a comprehensive study of its photocatalytic of Dyes and antibiotics, antibacterial, and antimutagenic activities. J. Photochem. Photobiol. A: Chem. **443**, 114874 (2023)
24. Mohammed, Hamdi Ali; Eddine, Laouini Salah; Souhaila, Meneceur; Hasan, Gamil Gamal; Kir, Iman; Abdullah, Johar Amin Ahmed.: Green synthesis of SnO_2 nanoparticles from Laurus nobilis L. extract for enhanced gelatin-based films and CEF@ SnO2 for efficient antibacterial activity. Food Bioprocess Technol. (2023). https://doi.org/10.1007/s11947-023-03209-8
25. Abdullah, J.A.; Ahmed, M.-R.; Perez-Puyana, V.; Guerrero, A.; Romero, A.: Green synthesis of FexOy nanoparticles with potential antioxidant properties. Nanomaterials **12**, 2449 (2022). https://doi.org/10.3390/nano12142449
26. Abdullah, J.A.; Ahmed, V.-P.; Guerrero, A.; Romero, A.: Novel hybrid electrospun poly(ε-caprolactone) nanofibers containing

green and chemical magnetic iron oxide nanoparticles. J. Appl. Polym. Sci. (2023). https://doi.org/10.1002/app.54345
27. Abdullah, J.A.; Ahmed, M.J.; Rosado, A.G.; Romero, A.: Eco-friendly synthesis of ZnO-nanoparticles using Phoenix dactylifera L., polyphenols: physicochemical, microstructural, and functional assessment. New J. Chem. **47**, 4409–4417 (2023). https://doi.org/10.1039/D3NJ00131H
28. Abdullah, J.A.A.; Soltani, M.; Laouini, S.: Synthèse verte et caractérisation des nanoparticules d'oxyde de fer (Fe_2O_3) par l'extrait des feuilles de Phœnix Dactylifera.L et évaluation de leur activité catalytique. Université Echahid Hamma Lakhdar, El Oued (2017)
29. El-Seedi, H.R.; El-Shabasy, R.M.; Khalifa, S.A.; Saeed, A.; Shah, A.; Shah, R.; Guo, W.: Metal nanoparticles fabricated by green chemistry using natural extracts: biosynthesis, mechanisms, and applications. RSC Adv. **9**(42), 24539–24559 (2019)
30. Manjari, G.; Saran, S.; Arun, T.; Vijaya Bhaskara Rao, A.; Devipriya, S.P.: Catalytic and recyclability properties of phytogenic copper oxide nanoparticles derived from Aglaia elaeagnoidea flower extract. J. Saudi Chem. Soc. **21**, 610–618 (2017)
31. Rahuman, H.; Beevi, H.; Dhandapani, R.; Narayanan, S.; Palanivel, V.; Paramasivam, R.; Subbarayalu, R.; Thangavelu, S.; Muthupandian, S.: Medicinal plants mediated the green synthesis of silver nanoparticles and their biomedical applications. IET Nanobiotechnol. **16**, 115–144 (2022)
32. Eddine, Laouini Salah; Mohammed, Hamdi Ali; Salmi, Chaima; Souhaila, Meneceur; Hasan, Gamil Gamal; Alharthi, Fahad; Abdullah, Johar Amin Ahmed.: Biogenic synthesis of Fe_3O_4/NiO nanocomposites using Ocimum basilicum leaves for enhanced degradation of organic dyes and hydrogen evolution. J. Porous Mater. (2023). https://doi.org/10.1007/s10934-023-01509-0
33. Abdullah, J.A.; Ahmed, Álvaro Díaz.-G.; Law, J.Y.; Romero, A.; Franco, V.; Guerrero, A.: Sustainable nanomagnetism: investigating the influence of green synthesis and pH on iron oxide nanoparticles for enhanced biomedical applications. Polymers **15**, 3850 (2023). https://doi.org/10.3390/polym15183850
34. Abdullah, J.A.; Ahmed, J.J.; Benítez, A.G.; Romero, A.: Sustainable integration of zinc oxide nanoparticles: enhancing properties of poly(ε-caprolactone) electrospun nanofibers and cast films. Coatings **13**, 1665 (2023). https://doi.org/10.3390/coatings13101665
35. Alver, Ü.M.İT.; Tanrıverdi, A.; Akgül, Ö.: Hydrothermal preparation of ZnO electrodes synthesized from different precursors for electrochemical supercapacitors. Synth. Met. **211**, 30–34 (2016)
36. Lin, Y.-G.; Hsu, Y.-K.; Lin, Y.-C.; Chen, Y.-C.: Hierarchical Fe_2O_3 nanotube/nickel foam electrodes for electrochemical energy storage. Electrochim. Acta **216**, 287–294 (2016)
37. Cheng, J.P.; Liu, L.; Ma, K.Y.; Wang, X.; Li, Q.Q.; Wu, J.S.; Liu, F.: Hybrid nanomaterial of α-Co (OH) 2 nanosheets and few-layer graphene as an enhanced electrode material for supercapacitors. J. Colloid Interface Sci. **486**, 344–350 (2017)
38. Tuncel, D.; Ökte, A.N.: ZnO@ CuO derived from Cu-BTC for efficient UV-induced photocatalytic applications. Catal. Today **328**, 149–156 (2019)
39. Wojnarowicz, J.; Chudoba, T.; Lojkowski, W.: A review of microwave synthesis of zinc oxide nanomaterials: reactants, process parameters and morphologies. Nanomaterials **10**, 1086 (2020)
40. Samadi, M.; Zirak, M.; Naseri, A.; Kheirabadi, M.; Ebrahimi, M.; Moshfegh, A.Z.: Design and tailoring of one-dimensional ZnO nanomaterials for photocatalytic degradation of organic dyes: a review. Res. Chem. Intermed. **45**, 2197–2254 (2019)
41. Das, A.; Nikhil, S.K.; Nair, R.G.: Influence of surface morphology on photocatalytic performance of zinc oxide: a review. Nano-Struct. Nano-Objects **19**, 100353 (2019)
42. Ma, M.; Huang, Y.; Liu, J.; Liu, K.; Wang, Z.; Zhao, C.; Shengchun, Qu.; Wang, Z.: Engineering the photoelectrochemical behaviors of ZnO for efficient solar water splitting. J. Semicond. **41**, 91702 (2020)
43. Chang, J.; Waclawik, E.R.: Facet-controlled self-assembly of ZnO nanocrystals by non-hydrolytic aminolysis and their photodegradation activities. CrystEngComm **14**, 4041–4048 (2012)
44. Peng, Y.-K.; Edman Tsang, S.C.: Facet-dependent photocatalysis of nanosize semiconductive metal oxides and progress of their characterization. Nano Today **18**, 15–34 (2018)
45. Albiter, E.; Merlano, A.S.; Rojas, E.; Barrera-Andrade, J.M.; Salazar, Á.; Valenzuela, M.A.: Synthesis, characterization, and photocatalytic performance of ZnO–graphene nanocomposites: a review. J. Compos. Sci. **5**, 4 (2020)
46. Park, H.; Park, Y.; Kim, W.; Choi, W.: Surface modification of TiO_2 photocatalyst for environmental applications. J. Photochem. Photobiol. C: Photochem. Rev. **15**, 1–20 (2013)
47. Li, B.; Wang, Y.: Facile synthesis and photocatalytic activity of ZnO–CuO nanocomposite. Superlatt. Microstruct. **47**, 615–623 (2010)
48. Harish, S.; Archana, J.; Sabarinathan, M.; Navaneethan, M.; Nisha, K.D.; Ponnusamy, S.; Muthamizhchelvan, C.; Ikeda, H.; Aswal, D.K.; Hayakawa, Y.: Controlled structural and compositional characteristic of visible light active ZnO/CuO photocatalyst for the degradation of organic pollutant. Appl. Surface Sci. **418**, 103–112 (2017)
49. Moradi, M.; Hasanvandian, F.; Isari, A.A.; Hayati, F.; Kakavandi, B.; Setayesh, S.R.: CuO and ZnO co-anchored on g-C3N4 nanosheets as an affordable double Z-scheme nanocomposite for photocatalytic decontamination of amoxicillin. Appl. Catal. B Environ. **285**, 119838 (2021)
50. Frelek-Kozak, M.; Kurpaska, L.; Wyszkowska, E.; Jagielski, J.; Jozwik, I.; Chmielewski, M.: Evaluation of consolidation method on mechanical and structural properties of ODS RAF steel. Appl. Surface Sci. **446**, 215–221 (2018)
51. Hasanvandian, F.; Salmasi, M.Z.; Moradi, M.; Saei, S.F.; Kakavandi, B.; Setayesh, S.R.: Enhanced spatially coupling heterojunction assembled from $CuCo_2S_4$ yolk-shell hollow sphere capsulated by Bi-modified TiO_2 for highly efficient CO_2 photoreduction. Chem. Eng. J. **444**, 136493 (2022)
52. Verma, D.; Patel, R.P.; Verma, M.L.: Structural and optical properties of Dy3+ doped Sr_2SiO_4 phosphors. Mater. Sci. Pol. **37**, 55–64 (2019)
53. Abbasi, S.; Hasanpour, M.: The effect of pH on the photocatalytic degradation of methyl orange using decorated ZnO nanoparticles with SnO_2 nanoparticles. J. Mater. Sci. Mater. Electron. **28**, 1307–1314 (2017)
54. Kir, Iman; Laouini, Salah Eddine; Meneceur, Souhaila; Bouafia, Abderrhmane; Mohammed, Hamdi Ali Mohammed.: Biosynthesis and characterization of novel nanocomposite ZnO/$BaMg_2$ efficiency for high-speed adsorption of AZO dye. Biomass Conv. Bioref. (2023). https://doi.org/10.1007/s13399-023-03985-5
55. Trivedi, M.; Tallapragada, R.M.; Branton, A.; Trivedi, D.; Latiyal, O.; Jana S.: Influence of biofield treatment on physical and structural characteristics of barium oxide and zinc sulfide. *J. Lasers, Opt. Photon.* 2 (2015)
56. Muhammad, W.; Ullah, N.; Haroon, M.; Abbasi, B.H.: Optical, morphological and biological analysis of zinc oxide nanoparticles (ZnO NPs) using Papaver somniferum L. RSC Adv. **9**, 29541–29548 (2019)
57. Perera, W.P.T.D.; Dissanayake, R.K.; Ranatunga, U.I.; Hettiarachchi, N.M.; Perera, K.D.C.; Unagolla, J.M.; De Silva, R.T.; Pahalagedara, L.R.: Curcumin loaded zinc oxide nanoparticles for activity-enhanced antibacterial and anticancer applications. RSC Adv. **10**, 30785–30795 (2020)
58. Mohammed, Mohammed; Ali, Hamdi; Souhaila, Meneceur; Eddine, Laouini Salah; Hasan, Gamil Gamal; Kir, Iman; Mahboub,

Mohammed Sadok: A novel biosynthesis of MgO/PEG nanocomposite for organic pollutant removal from aqueous solutions under sunlight irradiation. Environ. Sci. Res. (2023). https://doi.org/10.1007/s11356-023-26422-6
59. Chang, T.; Li, Z.; Yun, G.; Jia, Y.; Yang, H.: Enhanced photocatalytic activity of ZnO/CuO nanocomposites synthesized by hydrothermal method. Nano-Micro Lett. **5**, 163–168 (2013)
60. Das, S.; Srivastava, V.C.: Hierarchical nanostructured ZnO-CuO nanocomposite and its photocatalytic activity. J. Nano Res. **35**, 21–26 (2016)
61. Taufik, A.; Saleh, R.: Synergistic effect between ternary iron–zinc–copper mixed oxides and graphene for photocatalytic water decontamination. Ceram. Int. **43**, 3510–3520 (2017)
62. Kir, I.; Laouini, S.E.; Meneceur, S.; Bouafia, A.; Mohammed, H.A.M.: Biosynthesis and characterization of novel nanocomposite ZnO/$BaMg_2$ efficiency for high-speed adsorption of AZO dye. Biomass Conv. Bioref. (2023). https://doi.org/10.1007/s13399-023-03985-5
63. He, Yi.; Jiang, D.B.; Chen, J.; Zhang, Y.X.: Evaluation of MnO2-templated iron oxide-coated diatomites for their catalytic performance in heterogeneous photo Fenton-like system. J. Hazard. Mater. **344**, 230–240 (2018)
64. Ayon, S.A.; Billah, M.M.; Nishat, S.S.; Kabir, A.: Enhanced photocatalytic activity of Ho3+ doped ZnO NPs synthesized by modified sol-gel method: an experimental and theoretical investigation. J. Alloys Compd. **856**, 158217 (2021)